

Electronic property and topological phase transition in a graphene/$CoBr_2$ heterostructure

Yuan-Xiu Qin(秦元秀), Sheng-Shi Li(李胜世), Wei-Xiao Ji(纪维霄), and Chang-Wen Zhang(张昌文)

Citation: Chin. Phys. B, 2024, 33 (**2**): 027901. DOI: 10.1088/1674-1056/ad0f8a
Journal homepage: http://cpb.iphy.ac.cn; http://iopscience.iop.org/cpb

What follows is a list of articles you may be interested in

Growth behaviors and emission properties of Co-deposited $MAPbI_3$ ultrathin films on MoS_2

Siwen You(游思雯), Ziyi Shao(邵子依), Xiao Guo(郭晓), Junjie Jiang(蒋俊杰), Jinxin Liu(刘金鑫), Kai Wang(王凯), Mingjun Li(李明君), Fangping Ouyang(欧阳方平), Chuyun Deng(邓楚芸), Fei Song(宋飞), Jiatao Sun(孙家涛), and Han Huang(黄寒)
Chin. Phys. B, 2023, 32 (**1**): 017901. DOI: 10.1088/1674-1056/ac8e9b

Photoemission oscillation in epitaxially grown van der Waals *β*-In_2Se_3/WS_2 heterobilayer bubbles

Jiyu Dong(董继宇), Kang Lin(林康), Congpu Mu(牟从普), Zhiyan Jia(贾智研), Jin Xu(徐瑾), Anmin Nie(聂安民), Bochong Wang(王博翀), Jianyong Xiang(向建勇), Fusheng Wen(温福昇), Kun Zhai(翟昆), Tianyu Xue(薛天宇), and Zhongyuan Liu(柳忠元)
Chin. Phys. B, 2021, 30 (**11**): 117901. DOI: 10.1088/1674-1056/ac272f

Transport properties of doped Bi_2Se_3 and Bi_2Te_3 topological insulators and heterostructures

Zhen-Hua Wang(王振华), Xuan P A Gao(高翾), Zhi-Dong Zhang(张志东)
Chin. Phys. B, 2018, 27 (**10**): 107901. DOI: 10.1088/1674-1056/27/10/107901

Graphene/Mo_2C heterostructure directly grown by chemical vapor deposition

Rongxuan Deng(邓荣轩), Haoran Zhang(张浩然), Yanhui Zhang(张燕辉), Zhiying Chen(陈志蓥), Yanping Sui(隋妍萍), Xiaoming Ge(葛晓明), Yijian Liang(梁逸俭), Shike Hu(胡诗珂), Guanghui Yu(于广辉), Da Jiang(姜达)
Chin. Phys. B, 2017, 26 (**6**): 067901. DOI: 10.1088/1674-1056/26/6/067901

In-situ spectroscopic studies and interfacial engineering on FeSe/oxide heterostructures: Insights on the interfacial superconductivity

Peng Rui (彭瑞), Xu Hai-Chao (徐海超), Feng Dong-Lai (封东来)
Chin. Phys. B, 2015, 24 (**11**): 117902. DOI: 10.1088/1674-1056/24/11/117902

Electronic property and topological phase transition in a graphene/$CoBr_2$ heterostructure

Yuan-Xiu Qin(秦元秀), Sheng-Shi Li(李胜世), Wei-Xiao Ji(纪维霄), and Chang-Wen Zhang(张昌文)†

School of Physics and Technology, Institute of Spintronics, University of Jinan, Jinan 250022, *China*

(Received 8 October 2023; revised manuscript received 24 November 2023; accepted manuscript online 24 November 2023)

Recently, significant experimental advancements in achieving topological phases have been reported in van der Waals (vdW) heterostructures involving graphene. Here, using first-principles calculations, we investigate graphene/$CoBr_2$ (Gr/$CoBr_2$) heterostructures and find that an enhancement of in-plane magnetic anisotropy (IMA) energy in monolayer $CoBr_2$ can be accomplished by reducing the interlayer distance of the vdW heterostructures. In addition, we clarify that the enhancement of IMA energy primarily results from two factors: one is the weakness of the Co-d_{xy} and Co-$d_{x^2-y^2}$ orbital hybridization and the other is the augmentation of the Co-d_{yz} and Co-d_{z^2} orbital hybridization. Meanwhile, calculation results suggest that the Kosterlitz–Thouless phase transition temperature (T_{KT}) of a 2D *XY* magnet Gr/$CoBr_2$ (23.8 K) is higher than that of a 2D *XY* monolayer $CoBr_2$ (1.35 K). By decreasing the interlayer distances, the proximity effect is more pronounced and band splitting appears. Moreover, by taking into account spin–orbit coupling, a band gap of approximately 14.3 meV and the quantum anomalous Hall effect (QAHE) are attained by decreasing the interlayer distance by 1.0 Å. Inspired by the above conclusions, we design a topological field transistor device model. Our results support that the vdW interlayer distance can be used to modulate the IMA energy and QAHE of materials, providing a pathway for the development of new low-power spintronic devices.

Keywords: van der Waals heterostructure, in-plane magnetic anisotropy energy, quantum anomalous Hall effect

PACS: 79.60.Jv, 75.30.Gw, 64.70.Tg **DOI:** 10.1088/1674-1056/ad0f8a

1. Introduction

Graphene, a pioneering two-dimensional (2D) hexagonal honeycomb lattice material, attracts a great deal of attention for its excellent electronic, mechanical and optical properties.[1–3] In particular, among graphene's many properties, its topological properties are of interest due to its potential application in spintronics.[4–6] Up to now, the theoretical exploration of self-supported graphene has been extensive, prompting a shift in focus to graphene applications and the hope of making breakthroughs in graphene-based devices.

The weak intrinsic spin–orbit coupling (SOC) and lack of an orbital band gap in graphene hinder its further application.[7–10] However, the emergence of 2D van der Waals (vdW) opens up possibilities for utilizing graphene in various applications. Due to its sensitivity to the interlayer distance, the proximity effect in 2D vdW heterostructures offers a controllable way to adjust the electronic band structure of materials.[11–19] Significantly, vdW monolayers, unconstrained by the limitations of lattice matching, can be readily assembled into vdW heterostructures with arbitrary designs.[20–25] Moreover, the accumulation and hybridization properties of heterostructures constructed of 2D vdW materials are higher than those of the corresponding monolayer.[26–31] For instance, according to a recent experiment, the intrinsic SOC of graphene on SiO_2 is determined to be 20 μeV, which is higher than the value for pristine graphene (12 μeV).[32,33] Furthermore, it has been reported that vdW heterostructures have been used to obtain significant progress in achieving topological phases in graphene such as graphene/CrI_3.[34–36] In vdW heterostructures, time-reversal symmetry is broken by the presence of magnetic exchange and, combined with SOC, results in and the quantum anomalous Hall effect (QAHE),[37–40] i.e., time-reversal symmetry protects topological edge states, leading to topological protection as determined by Chern numbers.[34,35,37,41,42] Noticeably, some low-power-consumption spintronic devices can be designed based on the tunable dissipationless chiral edge state.

As for devices, the uniaxial magnetic anisotropy also plays a significant role. Recently, research has demonstrated that manipulation of the interlayer spacing in vdW heterostructures can effectively regulate perpendicular magnetic anisotropy (PMA), as exemplified by the graphene/NiI_2 (Gr/NiI_2) system.[43] The PMA of NiI_2 is significantly enhanced by decreasing interlayer distance, which is conducive to realizing low-power spintronic devices.[43–47] In addition, 2D materials with in-plane magnetic anisotropy (IMA), such as 2D *XY* magnets $CoBr_2$ and $CrCl_3$, have many excellent properties and application prospects.[44,48–50] However, in comparison to PMA, IMA has received significantly less research attention. To explore the variation of IMA and QAHE by decreasing the interlayer distance of vdW, in this work, we provide a systematic theoretical analysis of the elec-

†Corresponding author. E-mail: ss_zhangchw@ujn.edu.cn

© 2024 Chinese Physical Society and IOP Publishing Ltd

tronic and magnetic structures in a Gr/$CoBr_2$ heterostructure from first-principles calculations. Studies show that the $CoBr_2$ monolayer is an intrinsically ferromagnetic (FM) semiconductor with IMA, belonging to the 2D *XY* magnet family with a Kosterlitz–Thouless phase transition temperature $(T_{KT}) = 23.8$ K.[49] By analyzing the magnetic anisotropy energy (MAE) and density of states (DOS), we find that the MAE increases as the interlayer distance of Gr/$CoBr_2$ decreases and IMA, enhanced due to the interaction of Co-d orbitals, is modified by its proximity to graphene. Remarkably, decreasing the interlayer distance can lead to exchange splitting and a gap in the electronic band structure of graphene. Naturally, we also evaluate the topological characteristics of Gr/$CoBr_2$ when taking the SOC into account and the findings reveal the existence of the QAHE. Moreover, we design a device that suggests a pathway for novel low-power spintronic devices.

2. Computational details

We performed first-principles calculations using density-functional theory as implemented in the Vienna *ab initio* simulation package.[51–53] The generalized gradient approximation (GGA) with the Perdew–Burke–Ernzerhof realization was adopted for the exchange–correlation functional.[54] Considering the solid Co 3d electronic correlation effect in $CoBr_2$, the GGA $+U$ method is adopted ($U = 5$ eV, $J = 0.0$ eV).[43,49,55–57] The cutoff energy for the plane-wave base expansion is set to 500 eV. It is good enough to sample with a Γ-center $11 \times 11 \times 1$ k-point grid for the Brillouin zone and a center $25 \times 25 \times 1$ grid for the magnetic anisotropy calculation. Naturally, the MAE is calculated based on the energy variations between the in-plane and out-of-plane spin direction after considering SOC. The convergence criterion of the parameter for energy is 10^{-6} eV, and the criterion also requires the Hellmann–Feynman force acting on each atom to be less than 10^{-3} eV/Å. The vacuum space is set to 25 Å in the z-axis direction, which is sufficient to avoid false interactions. The topological properties are calculated by the Wannier function method in the WANNIER90 package.[58,59]

3. Results and discussion

3.1. Pristine $CoBr_2$ and Gr/$CoBr_2$ heterostructure

The monolayer $CoBr_2$ is exfoliated from bulk $CoBr_2$ crystals, having a CdI_2-type layered structure, as shown in Figs. 1(a) and 1(b), in which a cobalt metal atom forms an octahedron with six bromine atoms.[60] The adjacent layers of monolayer $CoBr_2$ are stacked together by weak vdW force, like in graphene, but it is reported to be stable in mechanics and thermodynamics.[48,49] The structure shows $P\bar{3}m1$ (No. 164) symmetry with broken inversion symmetry. The lattice parameters of monolayer $CoBr_2$ are calculated to be $a = b = 3.80$ Å, and the band structure of the material [Fig. 1(c)] indicates that $CoBr_2$ is a semiconductor with a global large band gap of 2.80 eV, which agrees well with previous research.[49]

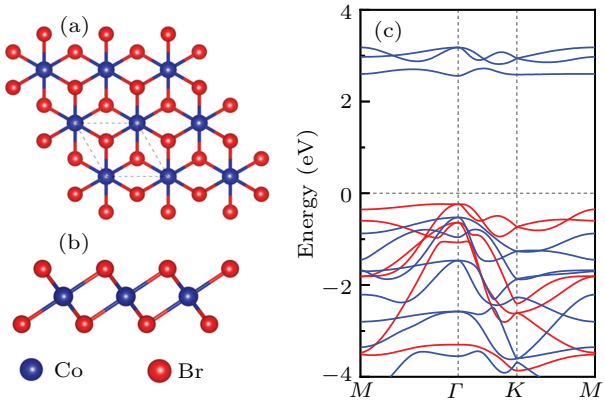


Fig. 1. (a) Top and (b) side views of the $CoBr_2$ monolayer. The primitive cell is marked by the dashed lines in (a). The blue and red balls represent Co and Br atoms, respectively. (c) Band structures of the $CoBr_2$ monolayer, E_g represents the band gap.

Considering that both $CoBr_2$ and graphene are vdW crystals, they can easily combine with each other. Here, the $3 \times 3 \times 1$ supercell of $CoBr_2$ is chosen as the substrate for the $5 \times 5 \times 1$ graphene for constructing a vdW heterostructure where graphene is stacked over the $CoBr_2$.[61–66] In Gr/$CoBr_2$, the interfacial Br atoms and the one on the other side are labeled by Br2 and Br1, respectively [Fig. 2(e)]. Since the interlayer interaction can be dependent on different stackings, we consider four high-symmetry configurations of Gr/$CoBr_2$ in Figs. 2(a)–2(d). In A1, the Co atom is on the hollow site of the C atom. In A2, the C atom is simply on top of the Co atom. In A3, the C atom is on top of the Br2 atom and, in A4, the C atom is on top of the Br1 atom. Our calculations find that A1 has the lowest energy and we focused on A1 in this study. The top and side views of A1 are shown in Fig. 2(a). The optimized lattice constant of Gr/$CoBr_2$ is 12.29 Å and interlayer binding energy is given by $E_b = [E(\text{Gr/CoBr}_2) - E(\text{CoBr}_2) - E(\text{graphene})]/a^2$. The distance between the two layers is 3.51 Å, with an interlayer binding energy of $E_b = -69.49$ meV/Å^2, where the interlayer distance suggests that the primary mode of interaction between the monolayers of graphene and $CoBr_2$ is a weak vdW force similar to other vdW heterostructures. Considering that the heterostructure is formed by stretching $CoBr_2$ in experiments, we simulate the impact on monolayer $CoBr_2$ of an external force during heterostructure formation and compute the phonon spectrum of the monolayer $CoBr_2$ under the 7.6% strain. In Fig. S1, the phonon spectrum of the $5 \times 5 \times 1$ supercell $CoBr_2$ has no imaginary frequency, which demonstrates that the $CoBr_2$ in the heterostructure is stable.

Next, in order to test the impact of the U value, we calculate the lattice constants and magnetic moments of each atom under different U values, as shown in Table 1. The results show that the lattice constants change slightly when the U value is varied from 2 eV to 5 eV. Moreover, in Fig. S2(a), we calculate the ground state based on a $2\times1\times1$ supercell of $Gr/CoBr_2$ according to the literature.[67] The FM and antiferromagnetic (AFM) energies (Figs. S2(b) and S2(c)) are calculated to identify the ground state of the $Gr/CoBr_2$ heterostructures. It is shown that the energy of the FM configuration is lower than that of the AFM configuration when $U = 5$ eV, $\Delta E = E_{AFM} - E_{FM} = 29.2$ meV, which shows that $Gr/CoBr_2$ presents an FM ground state in the same way as $CoBr_2$.

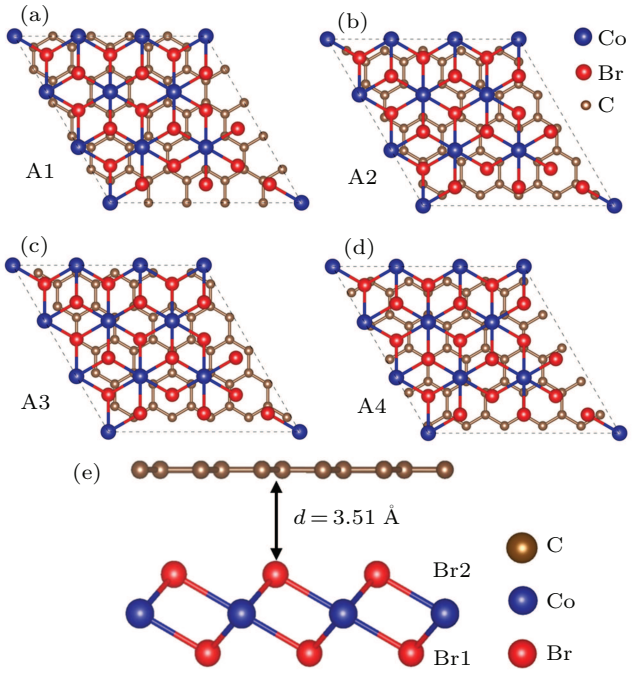


Fig. 2. (a)–(d) The top view of $Gr/CoBr_2$ heterostructures with A1, A2, A3 and A4 stackings. The brown spheres represent C atoms. (e) The side view of $Gr/CoBr_2$ heterostructure with A1 stackings.

Table 1. The lattice constants a, magnetic moments of Co m_{Co}, Br1 m_{Br1}, Br2 m_{Br2} and C m_c under different U values.

U (eV)	a (Å)	m_{Co} (μ_B)	m_{Br1} (μ_B)	m_{Br2} (μ_B)	m_c (μ_B)
2	12.30	2.560	0.140	0.135	0.00
3	12.30	2.615	0.123	0.120	0.00
4	12.30	2.667	0.106	0.105	0.00
5	12.29	2.727	0.084	0.083	0.00

3.2. Magnetic anisotropy tuned by interlayer spacing

$CoBr_2$ is a member of the 2D XY magnet family, i.e., it has an easy magnetic axis in the in-plane direction. Our calculation shows that the energy of the $CoBr_2$ monolayer is lowest when the electron spins along the in-plane direction, $\Delta E_{MAE} = E_x - E_z = -0.85$ meV, which accords with the above conclusion. The MAE of $Gr/CoBr_2$ when the easy magnetization axis is along the in-plane direction is shown in Fig. S3. Similarly, we investigate the MAE of 2D $Gr/CoBr_2$ when the SOC is included. In $Gr/CoBr_2$, we can calculate that $\Delta E_{MAE} = -8.17$ meV. The calculated result shows a preferred in-plane magnetization that is much larger than that of the monolayer $CoBr_2$. It is clear that the construction of $Gr/CoBr_2$ achieves the increase of MAE, providing a promising avenue for the development of spintronic devices.

Here, we choose $U = 5$ eV as an example to show the effect of the interlayer distance on MAE. In Fig. 3, we find that the IMA of Co atoms increases significantly with the decrease of interlayer distance, which ultimately causes an IMA increase of $Gr/CoBr_2$. In order to further explore the cause of MAE variation, we compare the orbit-resolved MAE between the Co atom in monolayer $CoBr_2$ and in a $Gr/CoBr_2$ heterostructure, as shown in Figs. 4(a)–4(c). From Fig. 4(a), one can clearly see that the contribution of in-plane magnetization is more evident than the out-of-plane magnetization of Co-d orbits in the pristine $CoBr_2$ monolayer. For the Co atom in pristine $CoBr_2$, the positive value of MAE is contributed by the hybridization between Co-$d_{x^2-y^2}$ and Co-d_{xy} (matrix element Co-$\langle d_{x^2-y^2}|\boldsymbol{L}_x|d_{xy}\rangle$), Co-$d_{yz}$ and Co-d_{xz} (matrix element Co-$\langle d_{yz}|\boldsymbol{L}_x|d_{xz}\rangle$); however, the negative value of MAE makes a significant hybridization contribution between Co-d_{z^2} and Co-d_{yz} (matrix element Co-$\langle d_{z^2}|\boldsymbol{L}_z|d_{yz}\rangle$). Therefore, the $CoBr_2$ monolayer presents characteristics of IMA.

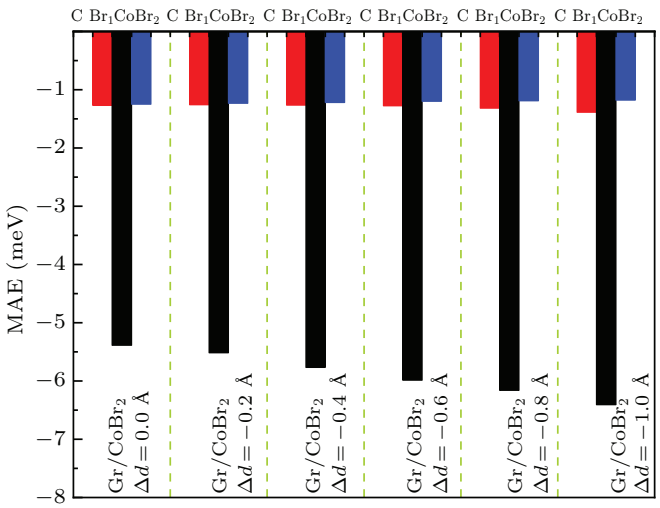


Fig. 3. The layer-resolved MAE of $Gr/CoBr_2$ with $\Delta d = 0.0$ Å, -0.2 Å, -0.4 Å, -0.6 Å, -0.8 Å and -1.0 Å, respectively.

After constructing $Gr/CoBr_2$ heterostructures, the attenuation of Co-$\langle d_{x^2-y^2}|\boldsymbol{L}_x|d_{xy}\rangle$ and the enhancement of Co-$\langle d_{yz}|\boldsymbol{L}_x|d_{xz}\rangle$ increase the IMA in Fig. 4(b). Similarly, in $Gr/CoBr_2$, we find that the IMA of Co atoms increases significantly with the decrease of interlayer distance, which causes the IMA increase of $Gr/CoBr_2$. Moreover, when the interlayer distance between graphene and $CoBr_2$ decreases by 1 Å, the weakening of the orbital hybridization between Co-d_{xy} and

Co-$d_{x^2-y^2}$ causes the IMA of Gr/$CoBr_2$ to increase remarkably, as shown in Fig. 4(c). In 2D materials, MAE can stabilize long-range FM order, withstanding the impact of thermal fluctuations. Naturally, MAE includes magnetocrystalline anisotropy (MCA) energy and magnetic shape anisotropy (MSA) energy, i.e., $E_{\mathrm{MAE}} = E_{\mathrm{MCA}} + E_{\mathrm{MSA}}$.[68] MSA is not considered in spin-density-based first-principles calculations. The MCA energy is related to the energy difference between the magnetization between the in-plane and out-of-plane direction relative to the $CoBr_2$ layer, $\Delta E_{\mathrm{MCA}} = E_{\mathrm{SOC}x} - E_{\mathrm{SOC}z}$.

$$E_{\mathrm{SOC}} = \left\langle \frac{h^2}{2m^2c^2}\frac{1}{r}\frac{\mathrm{d}V(r)}{\mathrm{d}r} \right\rangle \boldsymbol{L}\cdot\boldsymbol{S}, \tag{1}$$

where $\boldsymbol{L}$ represents the orbital angular momentum, $\boldsymbol{S}$ represents spin angular momentum and $V(r)$ is the spherical part related to the effective potential in projector augmented wave methodology.[69] MAE can be further expressed in the second-order perturbation theory as[70–72]

$$\begin{aligned}\Delta E^{--} &= E^{--}(x) - E^{--}(z)\\ &= \xi^2 o^- u^- \frac{|\langle o^-|\boldsymbol{L}_z|u^-\rangle|^2 - |\langle o^-|\boldsymbol{L}_x|u^-\rangle|^2}{E_u^- - E_o^-}, \qquad (2)\\ \Delta E^{+-} &= E^{+-}(x) - E^{+-}(z)\\ &= -\xi^2 o^+ u^- \frac{|\langle o^+|\boldsymbol{L}_z|u^-\rangle|^2 - |\langle o^+|\boldsymbol{L}_x|u^-\rangle|^2}{E_u^- - E_o^+}. \qquad (3)\end{aligned}$$

Here, ξ is the SOC constant, $+$ represents majority-spin states, $-$ represents minority-spin states, and E_u and E_o are the energy levels of the unoccupied and occupied states, respectively. The spin–orbital angular momentum matrix element differences, $|\langle o^-|\boldsymbol{L}_z|u^-\rangle|^2 - |\langle o^-|\boldsymbol{L}_x|u^-\rangle|^2$ and $|\langle o^+|\boldsymbol{L}_z|u^-\rangle|^2 - |\langle o^+|\boldsymbol{L}_x|u^-\rangle|^2$, in Eqs. (2) and (3) are illustrated in Table 2 for Co-d orbitals. Equations (2) and (3) show that the orbitals near the Fermi level are important components affecting the change of MAE. We can also see that the contributions of the same spin and opposite spin to MAE have opposite signs between the occupied and unoccupied states. In this case, the positive value of MAE means that the easy magnetization axis is perpendicular to the interface of monolayer $CoBr_2$. In contrast, the negative value implies an in-plane direction easy magnetic axis. To further investigate the mechanism of MAE change, in Figs. 4(d)–4(f), we plot the projected density of states (pDOS) of Co atoms in $CoBr_2$ and Gr/$CoBr_2$, respectively. It is found that both the occupied and the unoccupied electronic states of Co-d orbitals around E_{F} are mainly spin down in monolayer $CoBr_2$. Table 2 shows an element of -3 between spin-down occupied states d_{yz} ($d^{o^-}_{yz}$) and unoccupied d_{z^2} states ($d^{u^-}_{z^2}$) and an element of 4 between spin-down occupied $d_{x^2-y^2}$ states ($d^{o^-}_{x^2-y^2}$) and unoccupied d_{xy} states ($d^{u^-}_{xy}$), which induces the negative and positive MAE, respectively. However, it is obvious that the band around E_{F} is primarily contributed by d_{z^2} orbitals in Fig. 4(d); that is, the hybridization of d_{yz} and d_{z^2} induces the negative MAE contributions [grey bar in Fig. 4(a)]. Similarly, it can be seen from Figs. 4(e) and 4(f) that the $d^{o^-}_{yz}$ and the $d^{u^-}_{z^2}$ states make similar contributions to MAE, but the $d^{u^-}_{z^2}$ states are closer to the E_{F}, which means the states contribute more to MAE; meanwhile, the MAE contribution from the hybridization of $d^{o^-}_{x^2-y^2}$ and $d^{u^-}_{xy}$ keeps reducing when $CoBr_2$ approaches graphene, resulting in the enhancement of IMA in Gr/$CoBr_2$. In summary, graphene regulates the electronic states of Co atoms in Gr/$CoBr_2$ and enhances the IMA.

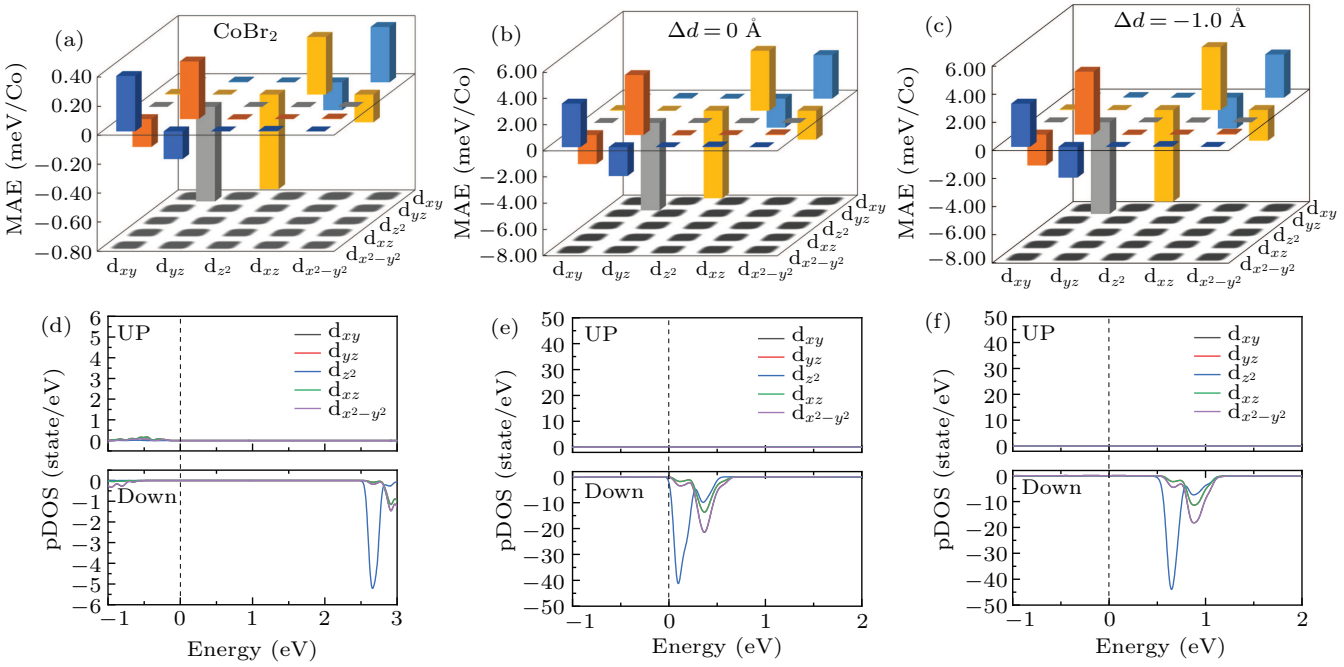


Fig. 4. MAE contributions from d-orbital hybridization of Co atoms in (a) pristine $CoBr_2$, Gr/$CoBr_2$ heterostructure with (b) $\Delta d = 0.0$ Å, (c) $\Delta d = -1.0$ Å. The pDOS of Co atom in (d) pristine $CoBr_2$, Gr/$CoBr_2$ heterostructure with (e) $\Delta d = 0$ Å, (f) $\Delta d = -1.0$ Å.

Our results of the MAE also show that the Gr/$CoBr_2$ heterostructures belong to the 2D *XY* magnet family. For 2D *XY* magnets, the finite size effect can be used to steady its magnetic order. In addition, the results show that the stability of the FM order in 2D *XY* magnets is strongly correlated with MAE. In order to demonstrate the effect of MAE on the magnetic transition temperature, we further determine the critical temperature T_{KT}.[73] According to the classical *XY* model, we estimate the critical temperature

$$T_{KT} = \pi J/2K_B, \tag{4}$$

where K_B is the Boltzmann constant and J is the exchange integral, which can be calculated from the exchange energy (ΔE)

$$J = \Delta E/(-2zS^2). \tag{5}$$

Here, S and z represent the spin of the Co atom and the number of nearest-neighboring Co atoms, respectively.

Considering only the first-nearest interactions, we obtain the nearest exchange integral $J_1 = 1.31$ meV and the T_{KT} is estimated to be 23.8 K. The T_{KT} of the $CoBr_2$ monolayer is calculated as 1.35 K, which is close to the previously reported value (1.7 K).[49] We discover that the transition temperature of the Gr/$CoBr_2$ is 17 times higher than that of the $CoBr_2$ monolayer. Therefore, the construction of the Gr/$CoBr_2$ heterostructure not only enhances the IMA of $CoBr_2$, but also effectively increases its critical temperature, which provides a theoretical basis for its development and application in the future.

Table 2. The matrix element differences of Co-d orbitals between two directions of the magnetization (z [001] and x [100]) in Eqs. (2) and (3).

u^-	o^+					o^-				
	d_{xy}	d_{yz}	d_{z^2}	d_{xz}	$d_{x^2-y^2}$	d_{xy}	d_{yz}	d_{z^2}	d_{xz}	$d_{x^2-y^2}$
d_{xy}	0	0	0	–1	4	0	0	0	1	–4
d_{yz}	0	0	–3	1	–1	0	0	3	–1	1
d_{z^2}	0	–3	0	0	0	1	–1	0	0	0
d_{xz}	–1	1	0	0	0	1	–1	0	0	0
$d_{x^2-y^2}$	4	–1	0	0	0	–4	1	0	0	0

3.3. Electronic properties and band structure of Gr/$CoBr_2$

In Fig. 5, we present the electronic band structures in the Gr/$CoBr_2$ heterostructure with an equilibrium interlayer distance of 3.51 Å. Figure 5(a) shows the representative electronic band structures without SOC of Gr/$CoBr_2$ with U = 5 eV, which indicates that the system is metallic and the Dirac cones of graphene are well preserved. When the SOC is considered, as shown in Figs. 5(b) and 5(c), we discover that the energy band opens up to a very small band gap (E_g = 6.25 meV).

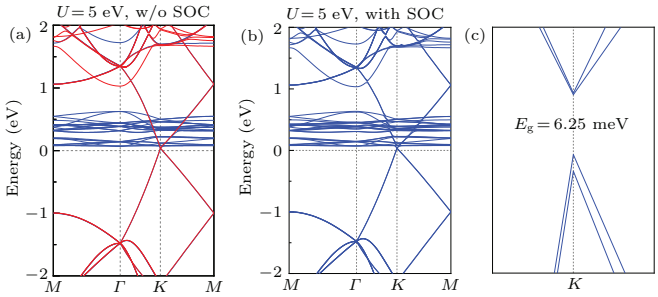


Fig. 5. (a) The energy band structures for the Gr/$CoBr_2$ heterostructure, with U values of 5 eV without considering the SOC. The red and blue lines represent spin-up and spin-down states, respectively. (b) Considering the SOC, the band structures with U values of 5 eV (c) Enlarged view of the band gap near the Fermi surface in (b).

Furthermore, in vdW heterostructures, it is proved that decreasing the interlayer distance can effectively tune the Dirac cones of graphene; hence, here we plot the band structure when the interlayer distance decreases by 0.2 Å to 1.0 Å, as shown in Figs. 6(a)–6(e). With decreasing interlayer distance, the opposite spin states are separated effectively by a strong magnetic exchange interaction, which produces significant exchange splitting when the interlayer distance is reduced to 2.51 Å, as shown in Figs. 6(e) and 6(f). Therefore, we choose U = 5 eV, d = 2.51 Å for the subsequent calculation of SOC in order to distinctly show the topological properties of Gr/$CoBr_2$.

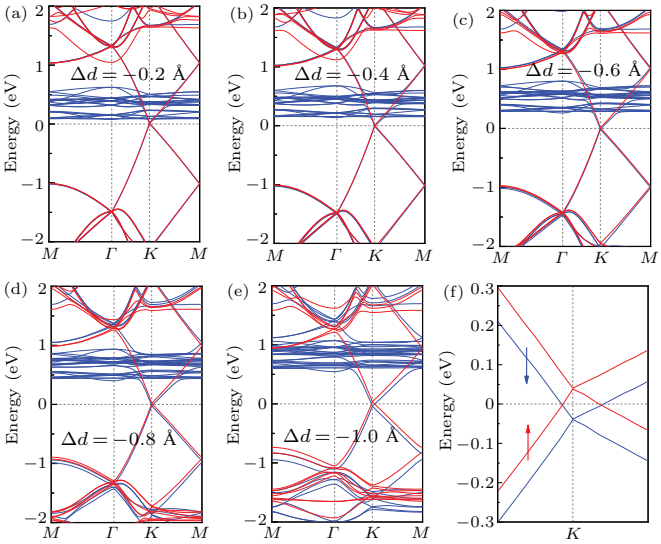


Fig. 6. (a)–(e) In the Gr/$CoBr_2$ heterostructure, the energy band structures with $\Delta d = -0.2$ Å, -0.4 Å, -0.6 Å, -0.8 Å and -1.0 Å, respectively. (f) Enlarged view of the black circle in (e).

3.4. Topological properties of the Gr/$CoBr_2$ heterostructure

A global band gap of $\sim$ 14.3 meV opens after SOC is switched on, where the E_F is right tuned to lie inside the

global gap, as shown in Figs. 7(a) and 7(b), indicating that the Gr/$CoBr_2$ heterostructure may harbor topologically nontrivial states.

Firstly, in order to analyse the cause of the QAHE, the theoretical model proposed by Ren *et al.* is employed in Gr/$CoBr_2$.[74] The tight-binding Hamiltonian with in-plane magnetization can be written as

$$H = -t\sum_{\langle ij\rangle} c_i^{\dagger}c_j + \mathrm{i}t_I \sum_{\langle\langle ij\rangle\rangle} v_{ij}c_i^{\dagger}s_z c_j - \mathrm{i}t_{\mathrm{IR}} \sum_{\langle\langle ij\rangle\rangle} \mu_{ij}c_i^{\dagger}\left(\boldsymbol{s}\times\hat{\boldsymbol{d}}_{ij}\right)_z c_j + \lambda\sum_i c_i^{\dagger}\hat{\boldsymbol{m}}\cdot\boldsymbol{s}c_i, \quad (6)$$

where $c_i^{\dagger} = (c_{i\uparrow}^{\dagger}, c_{i\downarrow}^{\dagger})^{\mathrm{T}}$ is the creation operator for an electron at the ith site and the $\uparrow$ ($\downarrow$) represents the spin-up (spin-down) state. The first term is the nearest-neighbor hopping and the second term is the intrinsic SOC, where t is the amplitude and $v_{ij} = \boldsymbol{d}_i \times \boldsymbol{d}_j / \left|\boldsymbol{d}_i \times \boldsymbol{d}_j\right|$ with $\boldsymbol{d}_{i,j}$ being the two nearest bonds connecting the next-nearest-neighbor sites. The third term represents the intrinsic-Rashba SOC H_{IR} where $\mu_{ij} = \pm 1$ for A/B sublattices, $\boldsymbol{s}$ are spin-Pauli matrices and $\hat{d}_{ij}$ is a unit vector from site j to i. The last term is the in-plane magnetization and λ and $\hat{\boldsymbol{m}} = (\cos\phi, \sin\phi, 0)$ are the strength and orientation, respectively.

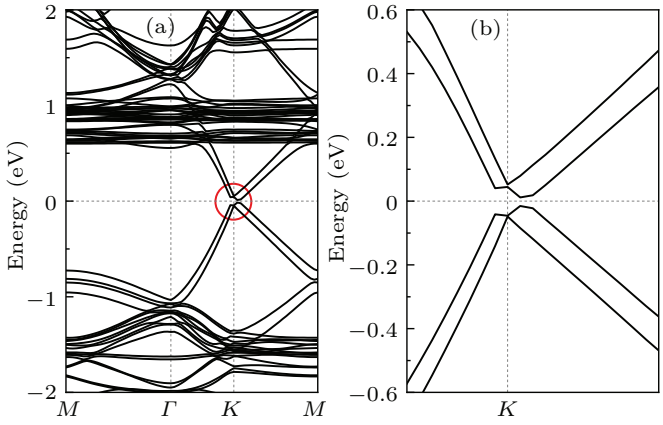


Fig. 7. (a) The band structure of Gr/$CoBr_2$ with $\Delta d = -1.0$ Å when SOC is included. (b) Enlarged view of the red circle in (a).

For Gr/$CoBr_2$, the broken symmetries of $\mathscr{T}\otimes\mathscr{M}_z\otimes\mathscr{I}$ (inversion $\mathscr{I}$, time reversal $\mathscr{T}$, out-of-plane mirror reflection $\mathscr{M}_z$) and $\mathscr{T}\otimes\mathscr{M}_z$ in 2D systems allow nonzero Chern numbers to occur, as expressed in references.[74–76] The emergence of magnetic substrates such as $CoBr_2$ and the construction of a supercell provide a possible pathway for the realization of the QAHE by decreasing the nearest-neighbor hopping energy. Once $\lambda > t$, the degeneracy is lifted, the band gap opens and the QAHE is characterized by Chern numbers of $C = 1$, which is consistent with the model.

To determine whether or not the resulting insulating state exhibits nontrivial topological properties, we evaluate the intrinsic anomalous Hall conductivity σ,

$$\sigma = \frac{e^2}{h}\frac{1}{2\pi}\int_{\mathrm{BZ}} \mathrm{d}^2\boldsymbol{k}\Omega(\boldsymbol{k}), \quad (7)$$

where e and h are the elementary charge and the Planck constant, respectively, the Berry curvature $\Omega(\boldsymbol{k})$ summed over occupied valence bands can be expressed by

$$\Omega(\boldsymbol{k}) = -2\,\mathrm{Im}\sum_n f_n \sum_{m\neq n} \frac{\langle\psi_{n\boldsymbol{k}}|v_x|\psi_{m\boldsymbol{k}}\rangle\langle\psi_{m\boldsymbol{k}}|v_y|\psi_{n\boldsymbol{k}}\rangle}{(E_m - E_n)^2}. \quad (8)$$

Here f_n is the Fermi–Dirac distribution function, v_x and v_y are the velocity operators, and E_n is the eigenvalue of the Bloch function $|\psi_{n\boldsymbol{k}}\rangle$.

Figure 8(a) shows the anomalous Hall conductivity σ_{xy}. We can see that σ_{xy} is quantized (e^2/h) as expected when the band gap of Gr/$CoBr_2$ contains a Fermi level. The result means the Chern number $C = 1$, which also can be obtained by the formula

$$C = \frac{1}{2\pi}\sum\nolimits_n \int_{\mathrm{BZ}} \mathrm{d}^2k\Omega_n. \quad (9)$$

The σ_{xy} rapidly reaches 0 as the Fermi level moves away from the band gap. Furthermore, the topological property of Gr/$CoBr_2$ is also estimated by the hybrid Wannier charge centers (WCCs) in Fig. 8(b). The electronic polarization WCC shifts with the winding number 1, which confirms the Chern number. Thus, it can be concluded that the Gr/$CoBr_2$ heterostructure harbors topologically nontrivial properties.

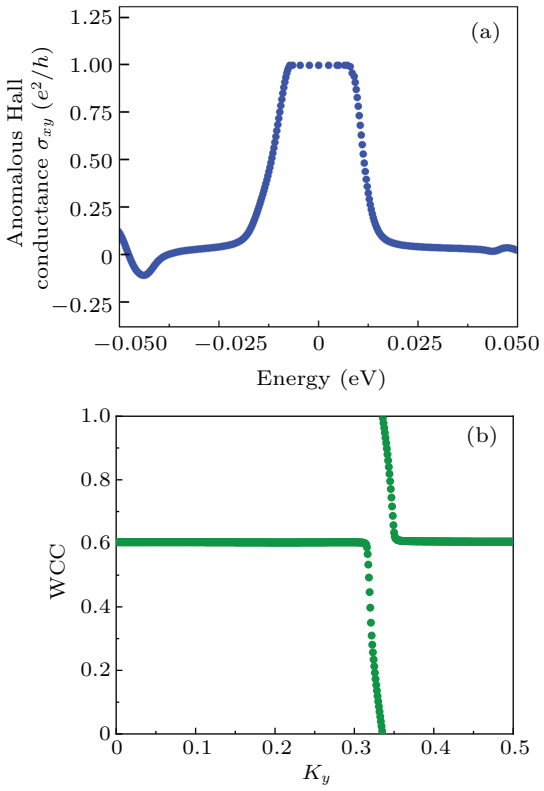


Fig. 8. (a) The anomalous Hall conductivity σ_{xy} and (b) the hybrid Wannier charge centers (WCCs).

Notably, the QAHE can be achieved by changing the interlayer distance. Based on this, we propose a conceptual

topological field-effect transistor that operates by switching the topological behavior of the Gr/$CoBr_2$ heterostructure on and off, as shown in Fig. 9. When the interlayer distance decreases by 1.0 Å, the device is in an 'on' state and the current will flow without dissipation in the edge states. In contrast, if the interlayer distance is not compressed, the device could be turned 'off' because of the lack of conductive channels. This study provides a new idea for the development of new spintronic devices with low-power consumption.

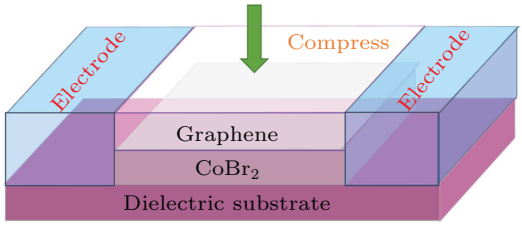


Fig. 9. Schematic diagram of the topological field transistor model.

4. Conclusion

In summary, we construct a Gr/$CoBr_2$ vdW heterostructure and predict its magnetic anisotropy and topological properties by first-principles calculations. The conclusion reveals that the Gr/$CoBr_2$ heterostructure is an FM semiconductor with IMA, belonging to the 2D XY magnet family with $T_{KT} = 23.8$ K. The MAE can be enhanced by decreasing the interlayer distance. However, the cause of MAE variation is the attenuation of Co-$\langle d_{x^2-y^2}|\boldsymbol{L}_x|d_{xy}\rangle$ and the enhancement of Co-$\langle d_{yz}|\boldsymbol{L}_x|d_{xz}\rangle$. The second-order perturbation theory shows that graphene can tune the electronic states of Co atoms, thereby enhancing the MAE arising by hybridization. Moreover, by analyzing the band structure, we elucidate that the decrease of interlayer distance produces a large exchange splitting in Gr/$CoBr_2$. After considering SOC, a global band gap of about 14.3 meV appears. Furthermore, anomalous Hall conductivity, a nonzero Chern number ($C = -1$) and WCC prove the topologically nontrivial property of Gr/$CoBr_2$. Our findings demonstrate that adjusting the vdW layer distance can not only control the MAE of 2D FM materials, but also provide a new way to realize the QAHE. Finally, on this basis, we design a topological field-effect transistor model, which provides a new idea for the development of new low-power spintronic devices.

Acknowledgements

Project supported by the National Natural Science Foundation of China (Grant No. 52173283), Taishan Scholar Program of Shandong Province (Grant No. ts20190939), and Independent Cultivation Program of Innovation Team of Jinan City (Grant No. 2021GXRC043).

References

[1] Akinwande D, Brennan C J, Bunch J S, Egberts P, Felts J R, Gao H, Huang R, Kim J S, Li T, Li Y, Liechti K M, Lu N, Park H S, Reed E J, Wang P, Yakobson B I, Zhang T, Zhang Y W, Zhou Y and Zhu Y 2017 *Extreme Mech. Lett.* **13** 42
[2] Miro P, Audiffred M and Heine T 2014 *Chem. Soc. Rev.* **43** 6537
[3] Siahrostami S, Tsai C, Karamad M, Koitz R, Garcia-Melchor M, Bajdich M, Vojvodic A, Abild-Pedersen F, Norskov J K and Studt F 2016 *Catal. Lett.* **146** 1917
[4] Han W, Kawakami R K, Gmitra M and Fabian J 2014 *Nat. Nanotechnol.* **9** 794
[5] Ren Y, Qiao Z and Niu Q 2016 *Rep. Prog. Phys.* **79** 066501
[6] Yang S A 2016 *Spin* **6** 1640003
[7] Jia K, Dong X J, Li S S, Ji W X and Zhang C W 2023 *ACS Appl. Nano Mater.* **6** 14003
[8] Min H, Hill J E, Sinitsyn N A, Sahu B R, Kleinman L and MacDonald A H 2006 *Phys. Rev. B* **74** 165310
[9] Yao Y, Ye F, Qi X L, Zhang S C and Fang Z 2007 *Phys. Rev. B* **75** 041401
[10] Zollner K, Faria P E Jr and Fabian J 2019 *Phys. Rev. B* **100** 085128
[11] Cardoso C, Soriano D, Garcia-Martinez N A and Fernandez-Rossier J 2018 *Phys. Rev. Lett.* **121** 067701
[12] Hallal A, Ibrahim F, Yang H, Roche S and Chshiev M 2017 *2D Materials* **4** 025074
[13] Khokhriakov D, Cummings A W, Song K, Vila M, Karpiak B, Dankert A, Roche S and Dash S P 2018 *Sci. Adv.* **4** eaat9349
[14] Qiao Z, Ren W, Chen H, Bellaiche L, Zhang Z, MacDonald A H and Niu Q 2014 *Phys. Rev. Lett.* **112** 116404
[15] Zollner K, Gmitra M, Frank T and Fabian J 2016 *Phys. Rev. B* **94** 155441
[16] Ci P, Chen Y, Kang J, Suzuki R, Choe H S, Suh J, Ko C, Park T, Shen K, Iwasa Y, Tongay S, Ager J W, III, Wang L W and Wu J 2017 *Nano Lett.* **17** 4982
[17] Gong C, Kim E M, Wang Y, Lee G and Zhang X 2019 *Nat. Commun.* **10** 2657
[18] Song T, Fei Z, Yankowitz M, Lin Z, Jiang Q, Hwangbo K, Zhang Q, Sun B, Taniguchi T, Watanabe K, McGuire M A, Graf D, Cao T, Chu J-H, Cobden D H, Dean C R, Xiao D and Xu X 2019 *Nat. Mater.* **18** 1298
[19] Yao W, Wang E, Bao C, Zhang Y, Zhang K, Bao K, Chan C K, Chen C, Avila J, Asensio M C, Zhu J and Zhou S 2018 *Proc. Natl. Acad. Sci. USA* **115** 6928
[20] Alexeev E M, Ruiz-Tijerina D A, Danovich M, Hamer M J, Terry D J, Nayak P K, Ahn S, Pak S, Lee J, Sohn J I, Molas M R, Koperski M, Watanabe K, Taniguchi T, Novoselov K S, Gorbachev R V, Shin H S, Fal'ko V I and Tartakovskii A I 2019 *Nature* **567** 81
[21] Cao Y, Fatemi V, Fang S, Watanabe K, Taniguchi T, Kaxiras E and Jarillo-Herrero P 2018 *Nature* **556** 43
[22] Hunt B, Sanchez-Yamagishi J D, Young A F, Yankowitz M, LeRoy B J, Watanabe K, Taniguchi T, Moon P, Koshino M, Jarillo-Herrero P and Ashoori R C 2013 *Science* **340** 1427
[23] Han Y T, Ji W X, Wang P J, Li P and Zhang C W 2023 *Nanoscale* **15** 6830
[24] Li S S, Ji W X, Hu S J, Zhang C W and Yan S S 2017 *ACS Appl. Mater. Interfaces* **9** 41443
[25] Sun H, Li S S, Ji W X and Zhang C W 2022 *Phys. Rev. B* **105** 195112
[26] Jin C, Kim J, Utama M I B, Regan E C, Kleemann H, Cai H, Shen Y, Shinner M J, Sengupta A, Watanabe K, Taniguchi T, Tongay S, Zettl A and Wang F 2018 *Science* **360** 893
[27] Sharpe A L, Fox E J, Barnard A W, Finney J, Watanabe K, Taniguchi T, Kastner M A and Goldhaber-Gordon D 2019 *Science* **365** 605
[28] Yu H, Liu G B, Tang J, Xu X and Yao W 2017 *Sci. Adv.* **3** e1701696
[29] Wang Y P, Ji W X, Zhang C W, Li P, Zhang S F, Wang P J, Li S S and Yan S S 2017 *Appl. Phys. Lett.* **110** 213101
[30] Wu B, Song Y L, Ji W X, Wang P J, Zhang S F and Zhang C W 2023 *Phys. Rev. B* **107** 214419
[31] Zhang S J, Zhang C W, Zhang S F, Ji W X, Li P, Wang P J, Li S S and Yan S S 2017 *Phys. Rev. B* **96** 205433
[32] Gmitra M, Konschuh S, Ertler C, Ambrosch-Draxl C and Fabian J 2009 *Phys. Rev. B* **80** 235431
[33] Sichau J, Prada M, Anlauf T, Lyon T J, Bosnjak B, Tiemann L and Blick R H 2019 *Phys. Rev. Lett.* **122** 046403
[34] Zhang J, Zhao B, Yao Y and Yang Z 2015 *Phys. Rev. B* **92** 165418
[35] Qiao Z, Jiang H, Li X, Yao Y and Niu Q 2012 *Phys. Rev. B* **85** 115439

[36] Han Y, Yan Z, Li Z, Xu X, Zhang Z, Niu Q and Qiao Z 2023 *Phys. Rev. B* **107** 205412
[37] Su S, Barlas Y, Li J, Shi J and Lake R K 2017 *Phys. Rev. B* **95** 075418
[38] Zhang H S, Ning Y H, Yang W J, Zhang J Y, Zhang R Q and Xu X H 2019 *Phys. Chem. Chem. Phys.* **21** 17087
[39] Liu Z, Han Y, Ren Y, Niu Q and Qiao Z 2021 *Phys. Rev. B* **104** L121403
[40] Liu Z, Ren Y, Han Y, Niu Q and Qiao Z 2022 *Phys. Rev. B* **106** 195303
[41] Qiao Z, Yang S A, Feng W, Tse W K, Ding J, Yao Y, Wang J and Niu Q 2010 *Phys. Rev. B* **82** 161414
[42] Zanolli Z, Niu C, Bihlmayer G, Mokrousov Y, Mavropoulos P, Verstraete M J and Blügel S 2018 *Phys. Rev. B* **98** 155404
[43] Cui Q, Liang J, Yang B, Wang Z, Li P, Cui P and Yang H 2020 *Phys. Rev. B* **101** 214439
[44] Bedoya-Pinto A, Ji J R, Pandeya A K, Gargiani P, Valvidares M, Sessi P, Taylor J M, Radu F, Chang K and Parkin S S P 2021 *Science* **374** 616
[45] Honjo H, Ikeda S, Sato H, Sato S, Watanabe T, Miura S, Nasuno T, Noguchi Y, Yasuhira M, Tanigawa T, Koike H, Muraguchi M, Niwa M, Ito K, Ohno H and Endoh T 2016 *IEEE Trans. Magn.* **52** 1
[46] Kent A D 2010 *Nat. Mater.* **9** 699
[47] Jia K, Dong X J, Li S S, Ji W X and Zhang C W 2023 *Nanoscale* **15** 8395
[48] Chen P, Zou J Y and Liu B G 2017 *Phys. Chem. Chem. Phys.* **19** 13432
[49] Lv H Y, Lu W J, Luo X, Zhu X B and Sun Y P 2019 *Phys. Rev. B* **99** 134416
[50] Zhou Y, Lu H, Zu X and Gao F 2016 *Sci. Rep.* **6** 19407
[51] Blochl 1994 *Phys. Rev. B* **50** 17953
[52] Kresse and Furthmuller 1996 *Phys. Rev. B* **54** 11169
[53] Kresse and Hafner 1993 *Phys. Rev. B* **47** 558
[54] Perdew J P, Burke K and Ernzerhof M 1996 *Phys. Rev. Lett.* **77** 3865
[55] Anisimov V I, Zaanen J and Andersen O K 1991 *Phys. Rev. B* **44** 943
[56] Dudarev S L, Botton G A, Savrasov S Y, Humphreys C J and Sutton A P 1998 *Phys. Rev. B* **57** 1505
[57] Jabar A, Masrour R, Kadim G, Hamedoun M, Hourmatallah A, Benzakour N, Rezzouk A, Bouslykhane K and Kharbach J 2021 *Commun. Theor. Phys.* **73** 1663
[58] Mostofi A A, Yates J R, Pizzi G, Lee Y S, Souza I, Vanderbilt D and Marzari N 2014 *Comput. Phys. Commun.* **185** 2309
[59] Wang X, Yates J R, Souza I and Vanderbilt D 2006 *Phys. Rev. B* **74** 195118
[60] Wilkinson M K, Cable J W, Wollan E O and Koehler W C 1959 *Phys. Rev.* **113** 497
[61] Gabrys P A, Seo S E, Wang M X, Oh E, Macfarlane R J and Mirkin C A 2018 *Nano Lett.* **18** 579
[62] Horide T, Kametani F, Yoshioka S, Kitamura T and Matsumoto K 2017 *ACS Nano* **11** 1780
[63] Jin M, Zhang H, Wang J, Zhong X, Lu N, Li Z, Xie Z, Kim M J and Xia Y 2012 *ACS Nano* **6** 2566
[64] Langjahr P A, Lange F F, Wagner T and Rühle M 1998 *Acta Mater.* **46** 773
[65] Liu J and Zhang J 2020 *Chem. Rev.* **120** 2123
[66] Shelke V, Mazumdar D, Srinivasan G and Gupta A 2011 *J. Appl. Phys.* **109** 07D914
[67] Calderon C E, Plata J J, Toher C, Oses C, Levy O, Fornari M, Natan A, Mehl M J, Hart G, Nardelli M B and Curtarolo S 2015 *Comput. Mater. Sci.* **108** 233
[68] Tung J C and Guo G Y 2007 *Phys. Rev. B* **76** 094413
[69] Yan S, Qiao W, Jin D, Xu X, Mi W and Wang D 2021 *Phys. Rev. B* **103** 224432
[70] Chen W Z, Jiang L N, Yan Z R, Zhu Y, Wan C H and Han X F 2020 *Phys. Rev. B* **101** 144434
[71] Wang D S, Wu R and Freeman A J 1993 *Phys. Rev. B* **47** 14932
[72] Yang B S, Zhang J, Jiang L N, Chen W Z, Tang P, Zhang X G, Yan Y and Han X F 2017 *Phys. Rev. B* **95** 174424
[73] Kosterlitz J M and Thouless D J 1973 *J. Phys. C: Solid State Phys.* **6** 1181
[74] Ren Y, Zeng J, Deng X, Yang F, Pan H and Qiao Z 2016 *Phys. Rev. B* **94** 085411
[75] Ren Y, Qiao Z and Niu Q 2020 *Phys. Rev. Lett.* **124** 166804
[76] Zhong P, Ren Y, Han Y, Zhang L and Qiao Z 2017 *Phys. Rev. B* **96** 241103